ELSEVIER

Materials Science and Engineering A 460–461 (2007) 77–85

MATERIALS SCIENCE & ENGINEERING A

www.elsevier.com/locate/msea

# The effect of severe plastic deformation on precipitation in supersaturated Al–Zn–Mg alloys

J. Gubicza [a,*], I. Schiller [a], N.Q. Chinh [a], J. Illy [a], Z. Horita [b], T.G. Langdon [c]

[a] *Department of Materials Physics, Eötvös Loránd University, Budapest, P.O.B. 32, H-1518, Hungary*
[b] *Department of Materials Science and Engineering, Faculty of Engineering, Kyushu University, Fukuoka 819-0395, Japan*
[c] *Departments of Aerospace & Mechanical Engineering and Materials Science, University of Southern California, Los Angeles, CA 90089-1453, USA*

Received 25 August 2006; received in revised form 2 January 2007; accepted 4 January 2007

**Abstract**

Experiments were conducted to examine the influence of equal-channel angular pressing (ECAP) on the development of precipitation microstructures in two supersaturated Al–Zn–Mg alloys. The results show that ECAP leads to an ultrafine grain size with finely dispersed η precipitates. It is concluded that processing by ECAP promotes the precipitation processes because dislocations act as nucleation sites for precipitates. Spherical precipitates were observed in the alloys processed by ECAP whereas long rod-like precipitates were also observed after ageing without ECAP. Calculations show the yield strengths estimated from the characteristic parameters of the precipitation microstructure are in good agreement with the values determined by mechanical testing.


*Keywords:* Equal-channel angular pressing (ECAP); Aluminum alloys; Ageing; Ultrafine grained microstructure; Precipitation

## 1. Introduction

Severe plastic deformation (SPD) techniques are now widely applied for the production of ultrafine-grained (UFG) microstructures in bulk metals [1,2]. These procedures have the advantage of giving fully dense materials without the introduction of any contaminants. Of the various SPD processes now available, equal-channel angular pressing (ECAP) has received the most attention because it can be scaled fairly easily for the production of reasonably large billets [3,4]. In processing by ECAP, the sample is pressed through a die constrained within a channel which is bent through an abrupt angle typically close to 90°. This imposes a high strain on the sample so that a high dislocation density is introduced and these dislocations re-arrange to form subgrain or grain boundaries. Experiments show the UFG microstructures produced by ECAP generally exhibit high yield strengths when testing at ambient temperature by comparison with their coarse-grained counterparts [5].

From a practical point of view, investigations of ECAP processing of precipitation-hardened aluminum-based alloys is of considerable importance because of the potential for making use of these alloys in industrial applications. Some limited results are now available showing that the very high stresses induced in ECAP not only lead to the production of UFG microstructures but also significantly affect the sizes and distributions of any second-phase particles and precipitates contained within the matrix [6–18]. However, the results reported to date are limited and, in addition, it is anticipated the morphology of the precipitates will depend critically on the temperature used for the ECAP processing. The present investigation was initiated to evaluate the effect of performing ECAP at a high temperature on the microstructural evolution and the precipitate distributions in two different Al–Zn–Mg alloys. The pressing operation was conducted on supersaturated solid solutions and the microstructures were examined both after processing and in an aged condition without processing by ECAP. The results show the yield strength of the samples processed by ECAP correlate directly with the characteristic features of the as-processed microstructures.

## 2. Experimental materials and procedures

Billets of Al–4.8Zn–1.2Mg–0.14Zr and Al–5.7Zn–1.9Mg–0.35Cu (wt.%) alloys were processed by ECAP. Before processing, the materials were solution heat-treated for 30 min at

* Corresponding author. Tel.: +36 1 3722876; fax: +36 1 3722811.
*E-mail address:* gubicza@ludens.elte.hu (J. Gubicza).

0921-5093/$ – see front matter © 2007 Elsevier B.V. All rights reserved.
doi:10.1016/j.msea.2007.01.001

743 K and water-quenched in order to introduce supersaturated solid solutions. For reference, there are several earlier reports of the mechanical and precipitation properties of these alloys in the quenched condition in the absence of processing by ECAP [19–22]. All of the ECAP processing was started within a few minutes of the quenching. Cylindrical billets having diameters of 10 mm and lengths of 70 mm were pressed through an ECAP die at a constant displacement rate of ∼5 mm/s. The ECAP die had an internal angle between the two channels of 90° and an angle at the outer arc of curvature of ∼20°, where these angular values lead to an imposed strain of ∼1 on each separate pass through the die [23]. Each sample was pressed repetitively through a total of eight passes at a temperature of 473 K following route $B_C$ where the sample is rotated about the longitudinal axis by 90° in the same sense between each pass [24]. Owing to the relatively high temperature used for the ECAP, it is reasonable to anticipate that precipitates will form from the supersaturated solid solutions during the pressing operation. To precisely delineate the effect of ECAP on the occurrence of precipitation in these two alloys, additional specimens were also prepared from the quenched alloys by artificial ageing at the same temperature as for ECAP (473 K) and for essentially the same time (30 min).

Phase compositions of the alloys were determined by X-ray diffraction using a Philips X'pert powder diffractometer with a Cu anode. The microstructures after ECAP were examined using X-ray diffraction line profile analysis. The profiles of both the Al matrix and the precipitates were measured on the cross-sections of the billets after the final ECAP pass using a high-resolution rotating anode diffractometer (Nonius, FR591) and Cu $K\alpha_1$ radiation. The peak profiles were evaluated using the conventional Multiple Whole Profile (MWP) fitting procedure described in detail in other reports [25,26]. In this procedure, the Fourier coefficients of the experimental profiles are fitted by the product of the theoretical Fourier transforms of the size and strain peak profiles. The theoretical functions used in this fitting procedure are calculated on the basis of a model of the microstructure in which the crystallites are assumed to have a spherical shape and a log-normal size distribution. It is reasonably assumed in this procedure that the lattice strains are caused by the movement of dislocations. The procedure may be used to estimate the area-weighted mean crystallite size ($\langle x \rangle_{area}$) and the density of dislocations ($\rho$).

The microstructures were also investigated using a JEOL-200CX transmission electron microscope (TEM) operating at 200 kV. The TEM foils were taken from the approximate mid-point of each billet at the centre of the cross-sections perpendicular to the longitudinal axes following the final ECAP pass. Precipitation was also examined using differential scanning calorimetry (DSC) where the specimens, after either ECAP or artificially ageing, were heated at a rate of 10 K/min from 300 to 750 K in a Perkin-Elmer DSC2 calorimeter. The Vickers hardness was measured on the cross-sections of the billets using a load of 2 N and the yield strengths were taken as one-third of the hardness values.

## 3. Experimental results

### 3.1. Microstructures after ECAP or ageing

Figs. 1 and 2 show the X-ray diffraction patterns taken on the cross-sections of the Al–Zn–Mg–Cu and Al–Zn–Mg–Zr specimens, respectively, after (a) ECAP and (b) ageing. The two upper X-ray diffractograms in Figs. 1 and 2 show that $MgZn_2$ precipitates (η-phase particles) are formed during ECAP processing at 473 K but there are no reflections of the η precipitates for the aged Cu-containing sample shown in Fig. 1b. By contrast, the aged Al–Zn–Mg–Zr alloy shows very weak reflections of $MgZn_2$ in Fig. 2b. These observations demonstrate that the formation of the η-phase particles was promoted through ECAP. It is apparent also from inspection of Figs. 1b and 2b that the relative intensities of the *200* reflection of the matrix is much higher than the other peaks, thereby indicating the presence of a strong texture in the matrix of both aged specimens. This texture was developed during the preliminary casting and extrusion operations in forming the billets. Figs. 1b and 2b show that the texture diminishes during ECAP, probably because the initial grains are fragmented into smaller subgrains having different orientations.

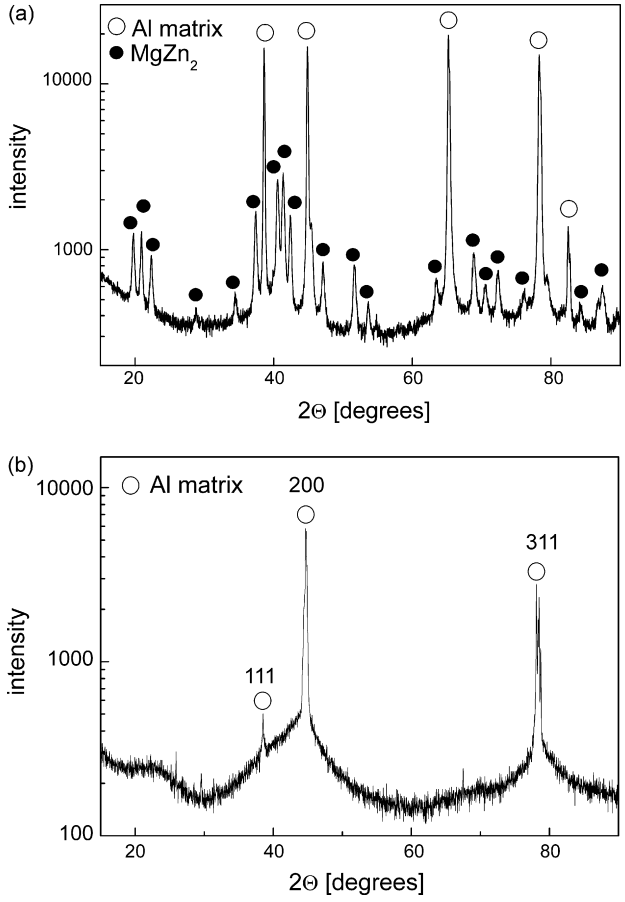


Fig. 1. X-ray diffractograms for the Al–Zn–Mg–Cu specimen (a) processed by ECAP and (b) aged at 473 K for 30 min: note the intensity is scaled logarithmically.

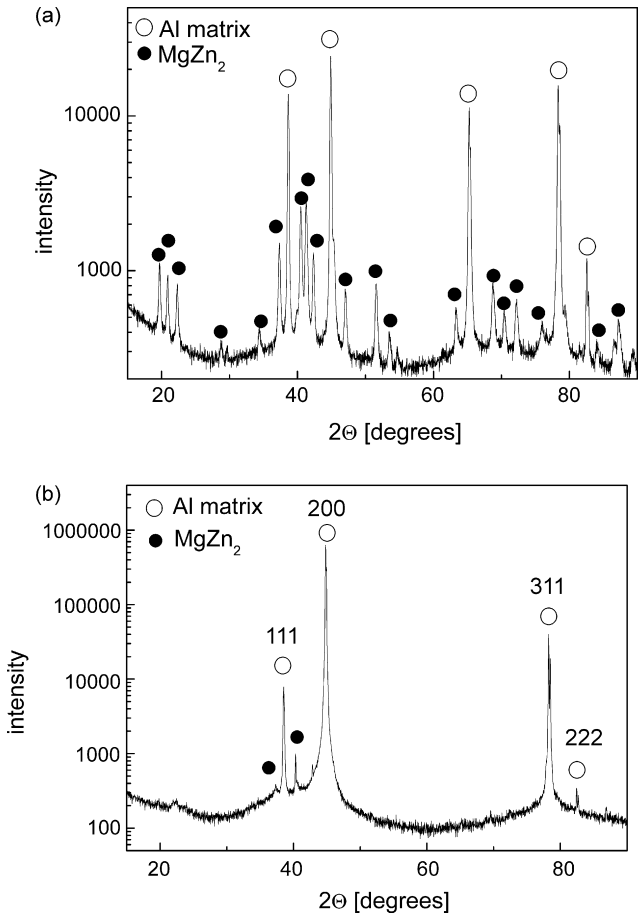


Fig. 2. X-ray diffractograms for the Al–Zn–Mg–Zr specimen (a) processed by ECAP and (b) aged at 473 K for 30 min: note the intensity is scaled logarithmically.

The line profiles of both the Al matrix and the η precipitates of the specimen processed by ECAP were evaluated using the MWP fitting procedure. Fig. 3 shows, for example, the Fourier coefficients of the measured intensity profiles (open circles) and the fitted theoretical Fourier transforms (solid line) for the Al matrix of the ECAP Al–Zn–Mg–Cu specimen. The difference between the measured and fitted values is also plotted. The area-weighted mean crystallite size and the dislocation density obtained from this fitting are summarized in Table 1. In practice, the very narrow peaks of the aged specimens make it impossible to use this line profile analysis for these samples.

Fig. 4 shows the *111*/*222* pair of X-ray line profiles of the Al matrix and the *00.2*/*00.4* reflections of the $MgZn_2$ precipitates for the Al–Zn–Mg–Cu specimen processed by ECAP. The

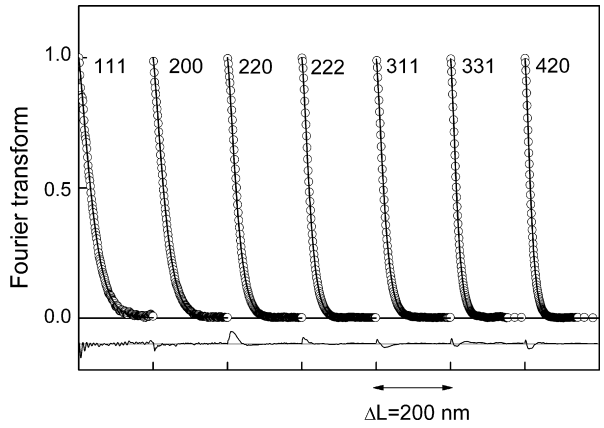


Fig. 3. The Fourier coefficients of the measured intensity profiles (open circles) and the fitted theoretical Fourier transforms (solid line) for the Al matrix of the ECAP Al–Zn–Mg–Cu specimen.

higher width of the *222* reflection compared to the *111* peak indicates unambigously the existence of strain broadening of the profiles for the Al matrix which is expressed by the dislocation density in the evaluation procedure. At the same time, the *00.2* and *00.4* reflections of the $MgZn_2$ phase are almost identical, indicating that the strain broadening of the line profiles for the η precipitates is negligible. A similar phenomenon was also observed for the Al–Zn–Mg–Zr alloy. As a consequence of the negligible strain broadening of the line profiles of the $MgZn_2$ phase, the dislocation structure of the precipitates was not evaluated from the diffraction peaks. However, the values of the area-weighted mean crystallite sizes obtained from the line profile analysis for the precipitates are also listed in Table 1.

The TEM micrographs shown in Fig. 5 are representative of the microstructures of (a) the Al–Zn–Mg–Zr and (b) the Al–Zn–Mg–Cu alloys, respectively, where both alloys were processed by ECAP. In both materials there is direct evidence for the formation of spherical precipitates during ECAP. The average sizes of these particles were measured as ∼30 and ∼20 nm for the Al–Zn–Mg–Zr and Al–Zn–Mg–Cu alloy, respectively. In addition, the average distance, *l*, between the particles was determined as ∼120 nm in the Al–Zn–Mg–Zr alloy and ∼80 nm in the Al–Zn–Mg–Cu alloy and the grain sizes of the matrices after ECAP were measured as ∼500 nm and ∼300 nm for Al–Zn–Mg–Zr and Al–Zn–Mg–Cu, respectively.

Fig. 6 shows TEM micrographs of the microstructures of the aged samples for (a) Al–Zn–Mg–Zr and (b) Al–Zn–Mg–Cu. It can be seen that the aged Al–Zn–Mg–Zr alloy contains both spherical and long rod-like precipitates in the interiors

Table 1
The grain size obtained from the TEM images ($d_{TEM}$), the area-weighted mean crystallite size ($\langle x \rangle_{area}$) and the dislocation density ($\rho$) determined from X-ray line profile analysis and the yield strength ($\sigma_Y$) for the Al–Zn–Mg–Zr and Al–Zn–Mg–Cu alloys

| Alloy | Phase | $d_{TEM}$ (nm) | $\langle x \rangle_{area}$ (nm) | $\rho$ ($10^{14}$ m$^{-2}$) | $\sigma_Y$ (MPa) |
|---|---|---|---|---|---|
| Al–Zn–Mg–Zr | Matrix | 500 | 165 ± 15 | 3.2 ± 0.4 | 290 ± 10 |
| | $MgZn_2$ | 30 | 30 ± 3 | – | |
| Al–Zn–Mg–Cu | Matrix | 300 | 119 ± 14 | 3.4 ± 0.4 | 380 ± 10 |
| | $MgZn_2$ | 20 | 22 ± 2 | – | |

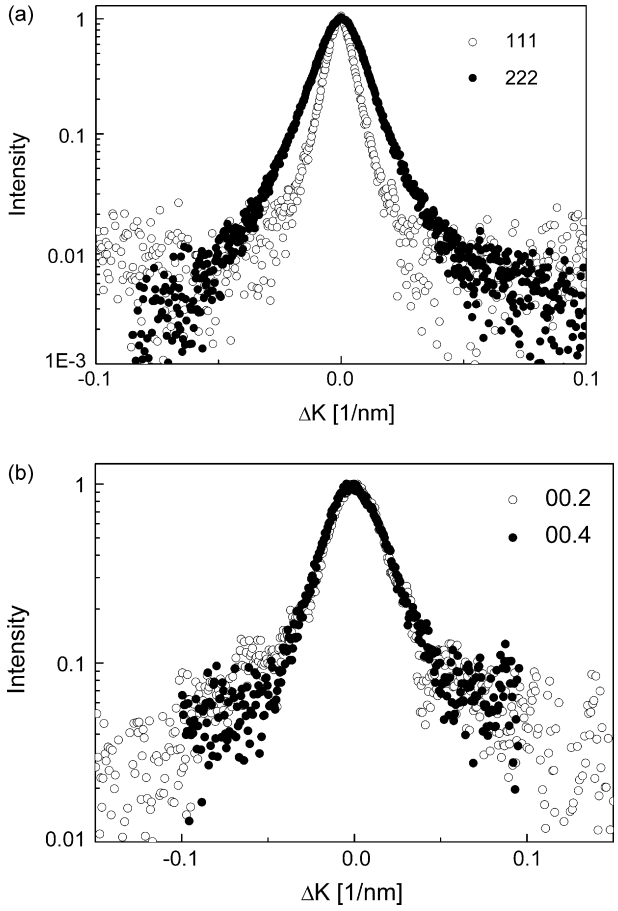


Fig. 4. (a) The *111/222* pair of X-ray line profiles of the Al matrix and (b) the *00.2/00.4* reflections of $MgZn_2$ precipitates for the Al–Zn–Mg–Cu alloy processed by ECAP.

of the grains. The size of these spherical particles is ∼30 nm while the diameters and lengths of the rod-like precipitates varied between ∼10–30 and ∼100–200 nm, respectively. For the Al–Zn–Mg–Cu alloy shown in Fig. 6b, the relative fraction of precipitates having sizes of ∼30 nm is very low and this explains the absence of the $MgZn_2$ reflections in the diffractogram of Fig. 1b. It should be noted that the TEM results also support the conclusions from the X-ray analysis regarding the influence of ECAP on the precipitation processes.

### *3.2. DSC analysis of alloys processed by ECAP or after ageing*

Fig. 7 shows the DSC thermograms recorded for (a) the Al–Zn–Mg–Zr alloy and (b) the Al–Zn–Mg–Cu alloy after ECAP and after ageing without ECAP. For both aged specimens, there are three characteristic peaks that are easily identified. The first endothermic peak between 330 and 430 K corresponds to the dissolution of the GP zones. The exothermic peak between 430 and 550 K relates to the formation of η'/η precipitates while the second endothermic peak between 550 and 650 K is due to precipitate dissolution. By contrast, the first two peaks are missing from the DSC thermograms for the specimens of the two alloys

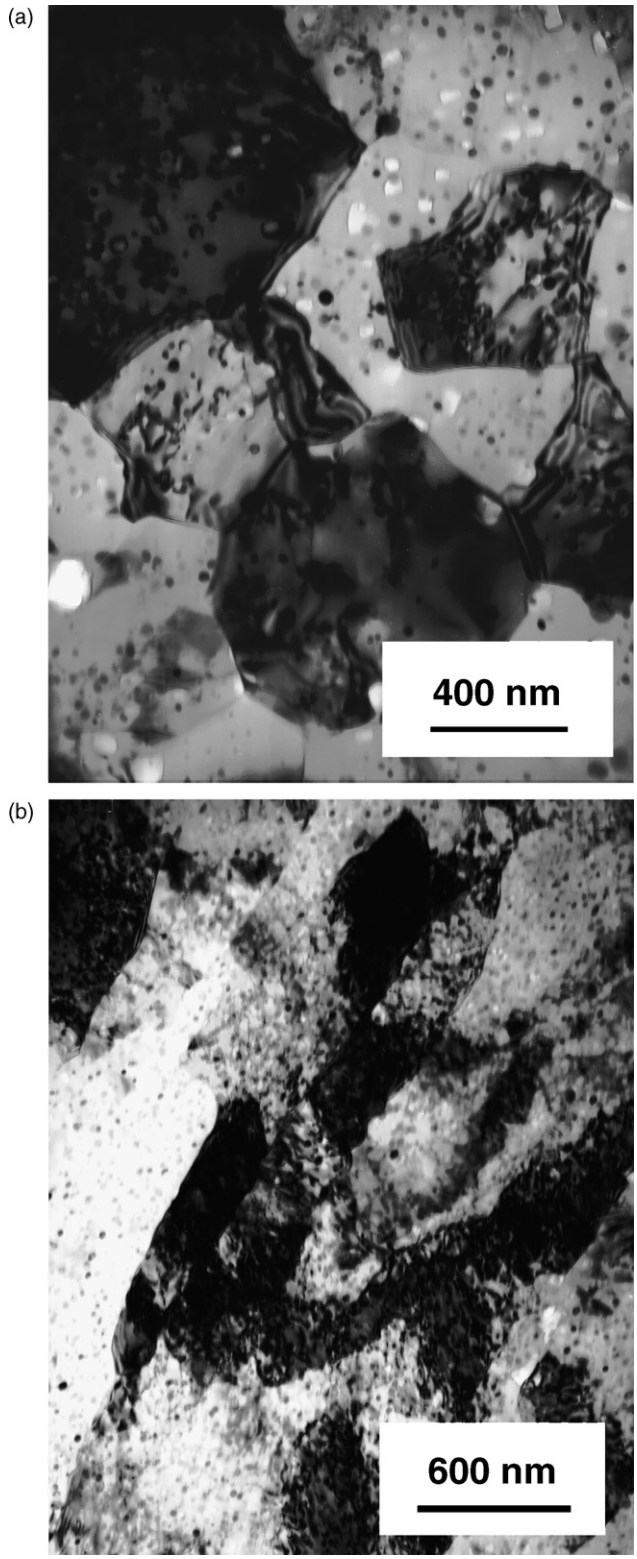


Fig. 5. Microstructures of (a) the Al–Zn–Mg–Zr alloy and (b) the Al–Zn–Mg–Cu alloy after ECAP.

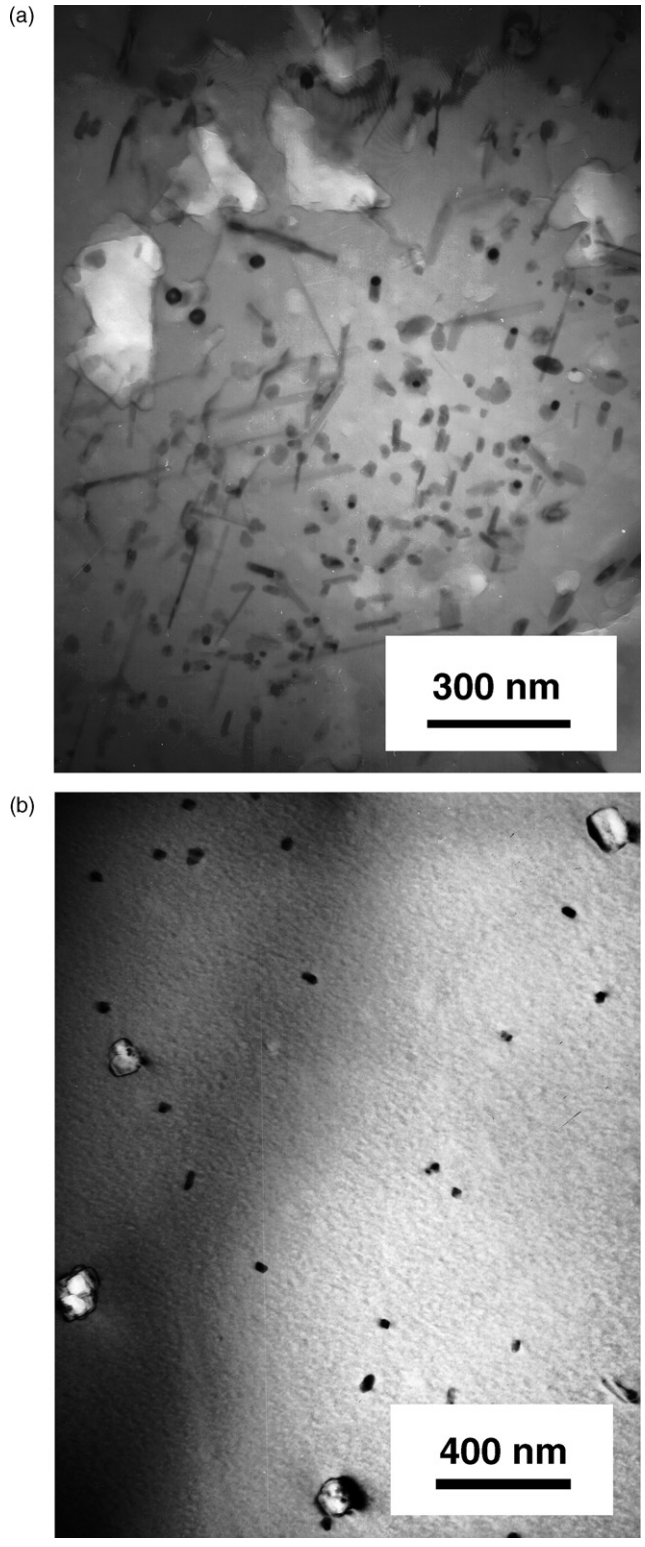


Fig. 6. Microstructures of (a) the Al–Zn–Mg–Zr alloy and (b) the Al–Zn–Mg–Cu alloy after ageing at 473 K for 30 min.

processed by ECAP, thereby showing that processing by ECAP gives a structure containing η precipitates without the presence of GP zones. This observation also confirms that ECAP has a very significant influence on the precipitation characteristics in these two aluminum-based alloys. The characteristic values of

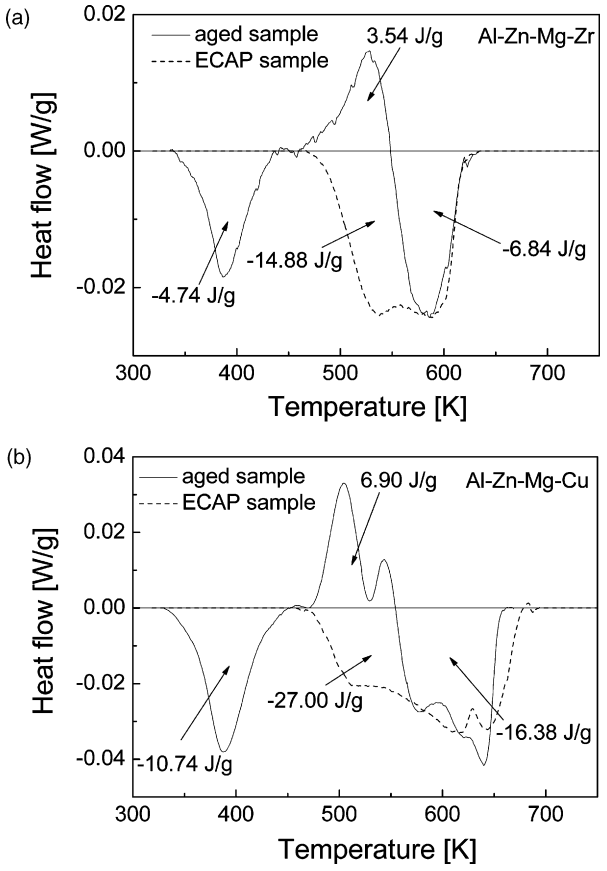


Fig. 7. DSC thermograms recorded at 10 K/min for (a) the Al–Zn–Mg–Zr alloy and (b) the Al–Zn–Mg–Cu alloy after ageing or processing by ECAP.

the areas under the DSC peaks calculated for mass unity are also included in Fig. 7.

### 3.3. Yield strength estimated from the hardness measurements

The yield strengths in the ECAP and aged conditions were estimated as one-third of the Vickers hardness values. Thus, the yield strengths are 290 ± 10 and 380 ± 10 MPa for the ECAP processed Al–Zn–Mg–Zr and Al–Zn–Mg–Cu alloys, respectively: these estimates are also included in Table 1. After artificial ageing at 473 K for 30 min, the values of the yield strength were 173 ± 8 and 182 ± 9 MPa for the Al–Zn–Mg–Zr and Al–Zn–Mg–Cu alloys, respectively. During storage of the samples at room temperature, natural ageing occurs in the aged samples so that the yield strength of the samples will increase with increasing ageing time. Fig. 8 shows the variation of the yield strength with the ageing time up to a maximum of 7 days at room temperature (RT) for the two aged alloys and the broken horizontal lines denote the estimated values of the yield strength for the ECAP specimens. Thus, the yield strength of the aged samples increases with increasing ageing time and this is attributed to the formation of GP zones during natural ageing at room temperature. After approximately 1 week of ageing at room temperature, the yield strengths of the aged samples reach saturation values of 295 ± 12 and

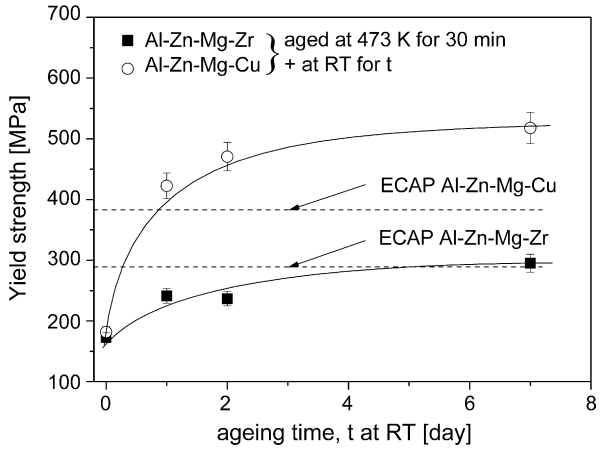


Fig. 8. The yield strength as a function of the natural ageing time at room temperature for the Al–Zn–Mg–Zr alloy and the Al–Zn–Mg–Cu alloy following ageing at 473 K for 30 min.

518 ± 20 MPa for the Al–Zn–Mg–Zr and Al–Zn–Mg–Cu alloys, respectively.

## 4. Discussion

### *4.1. The influence of ECAP on the precipitation microstructure*

The TEM micrographs in Figs. 5 and 6 provide a clear demonstration that processing by ECAP gives significant grain refinement in the matrices of the Al–Zn–Mg–Zr and Al–Zn–Mg–Cu alloys. As shown in Table 1, after ECAP processing the average grain sizes measured by TEM were in the range of ∼300–500 nm but these sizes are about 3-times higher than the mean crystallite sizes of ∼119–165 nm determined using X-ray analysis. This apparent discrepancy is now well-established in observations of materials processed by SPD and it is due to the subgrain structures and dislocation walls which form during SPD processing because these structural features are included within the estimates of the crystallite sizes when using the X-ray procedure [25]. Thus, the crystallite size determined from the X-ray line profiles corresponds essentially to the mean size of any subgrains or dislocation cells, and this mean size is generally smaller than the conventional grain size measured using TEM micrographs [25,27].

It is apparent from Table 1 that the sizes determined for the η precipitates are essentially identical using the TEM images and the X-ray analysis, thereby confirming that the $MgZn_2$ particles are in the form of single crystals without any additional substructural features. This latter observation and the absence of any strain broadening in the X-ray peaks of the $MgZn_2$ particles shown in Fig. 4b suggest that the η precipitates are not cut by the moving dislocations but instead the dislocations pass around the η particles by the bypass or Orowan mechanisms. Although the shearing of a precipitate does not necessarily leave dislocations within the particle, it is most probable that a cutting action would lead to dislocations remaining within a considerable fraction of the sheared precipitates thereby producing a measurable strain broadening of the X-ray profiles. Furthermore, no shearing of any precipitates is visible in the TEM images for the specimens processed by ECAP (see Fig. 5). This conclusion is fully consistent with the well-known incoherency of η particles within the matrix [28,29].

The simultaneous application of X-ray diffraction, TEM and DSC in the present investigation provides a direct confirmation that processing by ECAP strongly promotes the formation of precipitates in the two supersaturated Al–Zn–Mg alloys. This effect is revealed both by X-rays and TEM where the results demonstrate a higher concentration of η precipitates after ECAP by comparison with the same alloys in an undeformed condition but aged under the same thermal conditions. Moreover, the DSC thermograms reveal high fractions of GP zones in the aged alloys whereas GP zones were not detected after ECAP.

The effect of ECAP in promoting the formation of precipitates is attributed, at least in part, to the high dislocation density since the dislocations act readily as nucleation sites for the η particles. This can be explained by the faster diffusion of alloying elements within the cores of the dislocations and by the larger space for the alloying atoms in the dilatational zones around the dislocations. In this respect it is relevant to note that earlier DSC measurements on an Al-7034 alloy processed by ECAP showed that the endothermic peak for the dissolution of GP zones was missing in the DSC thermogram as processing by ECAP promoted the formation of η precipitates [30]. Another DSC investigation also demonstrated that ECAP induced an accelerating effect on precipitation in an Al-7075 alloy [12].

Careful inspection of the thermograms in Fig. 7 shows that, for both alloy compositions, the endothermic peak associated with the dissolution of η'/η particles starts at a lower temperature in the ECAP sample by comparison with the sample in the aged condition. This is probably due to the smaller size of the η particles after ECAP because it is probable that these small (∼10 nm) η particles are less stable and consequently they are more easily dissolved at lower temperatures [30]. It is possible also that there is a similar partial dissolution of the smaller precipitates in the aged sample but detection is then obscured by the exothermic reaction due to the formation of the large η particles. The values of the areas under the DSC peaks for the Al–Zn–Mg–Cu alloy are about twice as large as those for the Al–Zn–Mg–Zr alloy in both the ECAP and aged conditions, thereby indicating a stronger precipitation process because of the higher concentration of alloying element in the Al–Zn–Mg–Cu alloy.

The experimental results show that processing by ECAP at a high temperature influences not only the precipitation kinetics but also there is a significant effect on the shape of the η precipitates. Fig. 6a shows that the aged Al–Zn–Mg–Zr specimen contains long rod-like precipitates but these are absent when the same alloy is processed by ECAP. It is interesting to compare these observations with a recent report in which a commercial Al–Zn–Mg–Cu (7075) alloy was processed by ECAP at room temperature, aged at room temperature for 30 days and then heated to 473 K at 10 K/min in a calorimeter [12]. It should be

noted that this latter procedure differs from the present experiments where ECAP was conducted at 473 K so that SPD and precipitation occurs in a single step. Nevertheless, it is instructive to note that ECAP and ageing at room temperature leads to needle-like precipitates [12] whereas the present experiments revealed the presence of only essentially spherical particles as shown in Fig. 5.

In the present investigation, the lack of needle-like particles is due to the dynamic ageing process. Thus, the η' phase nucleus is formed in the early stages during the first pass of ECAP at 473 K and this phase is sheared by the dislocations introduced subsequently by severe plastic deformation. The η' phase precipitates are formed primarily along the (1 1 0) planes and they are then sheared into smaller particles by dislocations moving on the most active (1 1 1) planes. This leads ultimately to the presence of small and rather spherical η-phase precipitates during ECAP at 473 K, as illustrated in Fig. 5. It is noted that these incoherent η precipitates cannot be cut by dislocations either during subsequent ECAP passes or in mechanical testing after the processing operation. This conclusion is supported by the absence of any strain broadening in the X-ray line profiles in Fig. 4 and by the excellent agreement between the crystallite size and the grain size of the precipitates as determined by X-ray line profile analysis and TEM.

### 4.2. Correlation between the yield strength and the characteristic parameters of the microstructure

When considering the strength of particle-hardened ultrafine-grained alloys, several different strengthening mechanisms must be examined [31]. In broad terms, these mechanisms are (i) the work-hardening process due to the interaction between dislocations within the matrix, (ii) the Hall–Petch effect related to the interaction between dislocations and the grain boundaries, (iii) solid solution hardening and (iv) precipitation strengthening. The first three of these mechanisms occur if the alloy is a solid solution and the fourth mechanism must be additionally taken into account if the material contains precipitates.

Recently, it was shown, for both pure Al and Al–Mg solid solutions processed by ECAP at room temperature [32], that the yield strength ($\sigma_y$) measured by mechanical testing agrees well with the strength values calculated from the dislocation density using the Taylor relationhip:

$$\sigma_y = \sigma_0 + \alpha M^T G b \rho^{1/2}, \quad (1)$$

where $\sigma_0$ is the friction stress, $\alpha$ a constant (taken as $\alpha = 0.33$), $G$ the shear modulus ($G = 26$ GPa), $b$ the Burgers vector ($b = 0.2865$ nm) and $M^T$ the Taylor factor (where $M^T = 3$ for untextured polycrystalline materials). This result suggests that, in determining the strength for ultrafine-grained Al alloys processed by SPD, the interaction between dislocations (the work-hardening term), the effects of the grain boundaries (the Hall–Petch term) and partially the effect of the solute atoms (solid solution hardening) can all be incorporated into the average dislocation density, $\rho$. For the effect of grain boundaries, it should be noted that grain refinement in SPD occurs by the re-arrangement of dislocations into subgrain boundaries and/or cell walls so that, as also suggested by others [33], the effect of these subgrain/grain boundaries on dislocation motion can be described simply by the interaction between dislocations. It is emphasized that the dislocation densities obtained by the X-ray line profile analysis and listed in Table 1 involve dislocations in both the cell interiors and the boundaries even if they are geometrically necessary dislocations. With reference to solid solution strengthening, the solute atoms may increase the strength either by partially pinning the dislocations and impeding their motion or by indirectly reducing the recovery of dislocation structure during deformation and thus enhancing the dislocation–dislocation interactions. The former effect is taken into account in $\sigma_0$ while the latter effect is incorporated into the dislocation density.

For the alloys used in the present investigation, it is necessary also to include precipitation strengthening. Making the reasonable assumption of a linear additivity of the different strengthening contributions, the yield strength is accordingly given by [34]:

$$\sigma_y = \sigma_0 + \alpha M^T G b \rho^{1/2} + 0.85 M^T \frac{Gb \ln(x/b)}{2\pi(l - x)}, \quad (2)$$

where $x$ is the average size of the precipitates and $l$ the inter-precipitate spacing. The third term in Eq. (2) is generally used for a characterization of strengthening by non-shearable particles as in the present alloys.

The different factors contributing to the yield strength were estimated from Eq. (2) using the values of $l$ and $x$ measured from the TEM micrographs and the dislocation density determined using the X-ray line profile analysis. The value of $\sigma_0$ was taken as 20 MPa based on direct measurements recorded earlier for pure Al [35]: it is believed this value is reasonable because the value of the lattice parameter for the matrix of the alloys obtained from the X-ray diffractograms is in agreement within experimental error with the value for pure Al. The estimated strength contributions from the dislocation density, represented by the second term in Eq. (2), are ~133 and ~137 MPa for the Al–Zn–Mg–Zr and Al–Zn–Mg–Cu alloys, respectively, where these values are very close because of the similar values for the dislocation densities recorded in Table 1. The dislocation–precipitation interaction represented by the third term in Eq. (2) gives ~156 and ~214 MPa for the Al–Zn–Mg–Zr and Al–Zn–Mg–Cu alloys, respectively, where the difference is due to the different size and dispersion of precipitates in the two alloys. It follows from inspection of Eq. (2) that for non-shearable particles, such as the η-phase precipitates, both a decrease in the interparticle spacing ($l$) and an increase in the precipitate size ($x$) produce greater impediments to dislocation movement [36]. In practice, however, the interparticle spacing plays a stronger role than the precipitate size. In the present investigation, since both the average size of the precipitates and the distance between the η particles is lower in the Al–Zn–Mg–Cu alloy than in the Al–Zn–Mg–Zr alloy by nearly the same factor of about two-thirds, the precipitate structure of the Cu-containing alloy has a higher strengthening effect. Accordingly, the sum of the three hardening components

in Eq. (2) gives total strengths of ~309 ± 20 and ~371 ± 25 MPa for the Al–Zn–Mg–Zr and Al–Zn–Mg–Cu alloys, respectively, and these predicted values are in good agreement with the values listed in Table 1 from mechanical testing of 290 ± 10 and 380 ± 10 MPa, respectively.

Finally, it should be noted from Fig. 8 that the yield strength of the Al–Zn–Mg–Cu alloy is much higher after ageing than after ECAP because the GP zones have a larger strengthening effect than the η precipitates [22]. By contrast, the yield strengths for the Al–Zn–Mg–Zr alloy are essentially the same, at least within the experimental error, in the aged and ECAP condition despite the fact that the microstructures in these two conditions are different. It seems likely that this agreement is fortuitous and is simply a consequence of an approximate equivalence between the hardening effects of the GP zones and the $MgZn_2$ precipitates in the aged sample and the sum of the various strengthening effects of dislocations in the matrix and finely dispersed η particles in the sample processed by ECAP.

## 5. Conclusions

1. Experiments were conducted to examine the effect of ECAP processing at a high temperature (473 K) on the evolution of precipitation microstructures in Al–Zn–Mg–Zr and Al–Zn–Mg–Cu supersaturated solid solutions. Following ECAP, both alloys had ultrafine-grained microstructures with grain sizes of ~300–500 nm and dislocation densities within the matrix of $\sim 3 \times 10^{14}\ m^{-2}$.
2. Processing by ECAP leads to the formation of finely dispersed and non-shearable η-phase precipitates. Agreement between the crystallite size from X-ray line profile analysis and the grain size from transmission electron microscopy shows there is no substructure in the η particles. These observations are consistent with the well-known incoherency of η precipitates in the matrix.
3. By simultaneously using X-ray diffraction, TEM and DSC, it is demonstrated that ECAP promotes precipitation at high temperatures. In specimens aged at 473 K without straining, GP zones and η'/η precipitates are formed; whereas in specimens processed by ECAP at 473 K, only η particles are present.
4. Processing by ECAP has a significant effect on the shape of the precipitates. Spherical η particles are formed in the specimens processed by ECAP whereas long rod-like precipitates are also observed after ageing.
5. Calculations show that the yield strengths calculated from the dislocation density and from the size and separation of precipitates are in good agreement with experimental values determined from mechanical testing. The yield strength of the aged Al–Zn–Mg–Cu sample is higher than for the specimen processed by ECAP because of the stronger hardening effect of the GP zones compared to the η precipitates.

## Acknowledgements

The work of JG and NQC was supported by the Hungarian Scientific Research Fund, OTKA, Grant Nos. F-047057, T-043247 and T-038048. One of the authors was supported by the National Science Foundation of the United States under Grant No. DMR-0243331 (TGL). JG is grateful for the support of a Bolyai Janos Research Scholarship of the Hungarian Academy of Sciences. ZH was supported by the Light Metals Educational Foundation of Japan.

## References

[1] R.Z. Valiev, R.K. Islamgaliev, I.V. Alexandrov, Prog. Mater. Sci. 45 (2000) 103–189.
[2] R.Z. Valiev, Y. Estrin, Z. Horita, T.G. Langdon, M.J. Zehetbauer, Y.T. Zhu, JOM 58 (4) (2006) 33–39.
[3] V.M. Segal, Mater. Sci. Eng. A 197 (1995) 157–164.
[4] R.Z. Valiev, T.G. Langdon, Prog. Mater. Sci. 5l (2006) 881–981.
[5] Z. Horita, T. Fujinami, M. Nemoto, T.G. Langdon, Metall. Mater. Trans. A 31 (2000) 691–701.
[6] O.N. Senkov, F.H. Froes, V.V. Stolyarov, R.Z. Valiev, J. Liu, Nanostruct. Mater. 10 (1998) 691–698.
[7] M. Murayama, K. Hono, Z. Horita, Mater. Trans. 40 (1999) 938–941.
[8] M. Murayama, Z. Horita, K. Hono, Acta Mater. 49 (2001) 21–29.
[9] J.K. Kim, H.G. Jeong, S.I. Hong, Y.S. Kim, W.J. Kim, Scripta Mater. 45 (2001) 901–907.
[10] K. Oh-ishi, Y. Hashi, A. Sadakata, K. Kaneko, Z. Horita, T.G. Langdon, Mater. Sci. Forum 396–402 (2002) 333–338.
[11] C. Xu, M. Furukawa, Z. Horita, T.G. Langdon, Acta Mater. 51 (2003) 6139–6149.
[12] Y.H. Zhao, X.Z. Liao, Z. Jin, R.Z. Valiev, Y.T. Zhu, Acta Mater. 52 (2004) 4589–4599.
[13] M.J. Starink, N. Gao, M. Furukawa, Z. Horita, C. Xu, T.G. Langdon, Rev. Adv. Mater. Sci. 7 (2004) 1–12.
[14] C. Xu, M. Furukawa, Z. Horita, T.G. Langdon, Acta Mater. 53 (2005) 749–758.
[15] M. Cabibbo, E. Evangelista, M. Vedani, Metall. Mater. Trans. A 36 (2005) 1353–1364.
[16] T. Fujita, S. Nishimura, T. Fujinami, K. Kaneko, Z. Horita, D.J. Smith, Mater. Sci. Eng. A 417 (2006) 149–157.
[17] I. Gutierrez-Urrutia, M.A. Muñoz-Morris, D.G. Morris, J. Mater. Res. 21 (2006) 329–342.
[18] Z. Zhang, S. Hosoda, I.-S. Kim, Y. Watanabe, Mater. Sci. Eng. A 425 (2006) 55–63.
[19] N.Q. Chinh, Zs. Kovács, L. Reich, F. Székely, J. Illy, J. Lendvai, Z. Metall. 88 (1997) 607–611.
[20] N.Q. Chinh, F. Csikor, J. Lendvai, Mater. Sci. Forum 332 (2000) 1007–1012.
[21] N.Q. Chinh, Gy. Horváth, Zs. Kovács, J. Lendvai, Mater. Sci. Eng. A 324 (2002) 219–224.
[22] N.Q. Chinh, J. Lendvai, D.H. Ping, K. Hono, J. Alloys Compd. 378 (2004) 52–60.
[23] Y. Iwahashi, J. Wang, Z. Horita, M. Nemoto, T.G. Langdon, Scripta Mater. 35 (1996) 143–146.
[24] M. Furukawa, Y. Iwahashi, Z. Horita, M. Nemoto, T.G. Langdon, Mater. Sci. Eng. A 257 (1998) 328–332.
[25] T. Ungár, J. Gubicza, G. Ribárik, A. Borbély, J. Appl. Cryst. 34 (2001) 298–310.
[26] G. Ribárik, T. Ungár, J. Gubicza, J. Appl. Cryst. 34 (2001) 669–676.
[27] J. Gubicza, N.Q. Chinh, Z. Horita, T.G. Langdon, Mater. Sci. Eng. A 387–389 (2004) 55–59.
[28] J.Q. Su, T.W. Nelson, R. Mishra, M. Mahoney, Acta Mater. 51 (2003) 713–729.
[29] L.F. Mondolfo, Int. Metall. Rev. 153 (1971) 95–124.
[30] N. Gao, M.J. Starink, M. Furukawa, Z. Horita, C. Xu, T.G. Langdon, Mater. Sci. Forum 503–504 (2006) 275–280.

[31] M.J. Starink, S.C. Wang, Acta Mater. 51 (2003) 5131–5150.
[32] J. Gubicza, N.Q. Chinh, Gy. Krállics, I. Schiller, T. Ungár, Curr. Appl. Phys. 6 (2006) 194–199.
[33] D.A. Hughes, N. Hansen, Acta Mater. 48 (2000) 2985–3004.
[34] U.F. Kocks, Phil. Mag. 13 (1966) 541–566.
[35] N.Q. Chinh, Gy. Horváth, Z. Horita, T.G. Langdon, Acta Mater. 52 (2004) 3555–3563.
[36] M.F. Ashby, Proceedings of the Second Bolton Landing Conference on Oxide Dispersion Strengthening, Gordon and Breach, New York, NY, 1968, pp. 119–128.